

# Structure of magnetic fields in NOAA active regions 0486 and 0501 and in the associated interplanetary ejecta

Vasyl Yurchyshyn

Big Bear Solar Observatory, 40386 North Shore Lane, Big Bear City, CA 92314, USA

Qiang Hu

IGPP, University of California, Riverside, CA 92521, USA

Valentyna Abramenko

Big Bear Solar Observatory, 40386 North Shore Lane, Big Bear City, CA 92314, USA  
Crimean Astrophysical Observatory, 98409, Nauchny, Crimea, Ukraine

## Abstract.

Spectacular burst of solar activity in October – November 2003, when large solar spots and intense solar flares dominated the solar surface for many consecutive days, caused intense geomagnetic storms. In this paper we analyze solar and interplanetary magnetic fields associated with the storms in October – November 2003. We used space and ground based data in order to compare the orientations of the magnetic fields on the solar surface and at 1AU as well as to estimate parameters of geomagnetic storms during this violent period of geomagnetic activity. Our study further supports earlier reports on the correlation between the CME speed and the strength of the magnetic field in an interplanetary ejecta. A good correspondence was also found between directions of the helical magnetic fields in interplanetary ejecta and in the source active regions. These findings are quite significant in terms of their potential to predict the severity of geomagnetic activity 1 – 2 days in advance, immediately after an earth-directed solar eruption.

## 1. Introduction

The unexpected and spectacular burst of solar activity in October – November 2003 associated with large sunspots and intense solar flares dominated the solar landscape for many consecutive days. Particle events and CMEs, associated with this enhanced period of solar activity, caused huge disturbances in the earth's magnetosphere (geomagnetic storms). In general, during such a storm, the enhanced ring current is formed and it greatly decreases the earth's magnetic field near-equatorial zones, which results in a significant electric potential on conductors in all kinds of operating systems. As more advanced and interconnected systems are employed, the effects of the upper atmosphere become more profound. Although most operational systems can resist the effect of certain levels of magnetospheric activity, large storms can still cause significant damage to space- and ground-based installations, such as satellites, long-line communication networks and electric power grids.

Thus auroras, associated with the October-November period of activity on the Sun, were seen as far to the equator as Florida, Texas and Australia; radio blackouts disrupted telecommunications; and about 59% of spacecraft in some degree were affected by the burst in geomagnetic activity (see *Barbieri and Mahmot* [2004] for more details on space weather during October – November 2003).

Geomagnetic storms are significant perturbations of the earth's magnetosphere that occur when the interplanetary magnetic field (IMF) turns southward ( $B_z < 0$ ) and remains so for a prolonged period of time (several hours or more) [*Rostoker and Fälthammar*, 1967; *Russell et al.*, 1974; *Gonzalez and Tsurutani*, 1987; *Gonzalez et al.*, 1994]. Reconnection between southward IMF and the northwardly directed geomagnetic field occurs at the day side magnetopause and this reconnection transports energy from the solar wind into the magnetosphere [*Dungey*, 1961]. This reconnection

stresses the earth magnetic field and the degree of the stress, the Dst index, is a measure of the intensity of a geomagnetic storm.

Shortly after they were discovered [*Tousey*, 1973; *MacQueen et al.*, 1974; *Gosling et al.*, 1974] it was found that the occurrence of geomagnetic storms is correlated with the eruption of earth directed (halo, *Howard et al.* [1982]) CMEs [*Burlaga et al.*, 1981; *Wilson and Hildner*, 1984], which are observed at 1AU as interplanetary CMEs (ICME). In some cases, though, attempts to associate geomagnetic storms with solar flares led researchers to a category of "problem storms" for which no clear (or too insignificant) associations were found to properly account for the magnitude of the geomagnetic events [*McAllister et al.*, 1996].

CMEs are the result of a large-scale rearrangement of the solar magnetic field (see *Low* [2001] for a review) and, when observed at 1AU, their magnetic structure can variously be described as complex ejecta [*Burlaga et al.*, 2001], magnetic clouds (MC, [*Burlaga et al.*, 1981; *Bothmer and Schwenn* 1998]), plasmoids or a shock, associated with twisted IMF, that has footpoints rooted in the sun and heliosphere [*Dryer* 1994].

*Gonzalez and Tsurutani* [1987] pointed out that intense storms ( $Dst \leq -100$  nT) were caused by intense southwardly directed magnetic fields, where  $B_z < -10$  nT. Later, *Cane et al.* [2000], *Wu and Lepping* [2002, 2005] and *Yurchyshyn et al.* [2003, 2004] found high correlation between the intensity of the  $B_z$ , and the Dst index.

The strength of the magnetic field in an ICME is determined by the initial conditions of the eruption as well as by how it interacts with the interplanetary medium during its travel toward the earth. While it is not clear how the magnitude of the magnetic field in a CME may be related to its speed, the compression of the plasma ahead of the ICME is expected to be related to its faster speed relative to the ambient solar wind. Indeed, *Dal Lago et al.* [2001] and *Owens and Cargill* [2002] reported on the relationship between the intensity of the field in magnetic clouds and their velocity. Earlier, *Lindsay et al.* [1999] concluded that instances of the IMF with larger maximum magnitudes are found to be associated with high speed CMEs. However, these authors did not find any regular trend

in the intensity of  $B_z$  as a function of the CME speed, which was explained by the fact that an ICME can have a different orientation with respect to the orbital plane of a satellite. *Yurchyshyn et al.* [2004] analyzed data for 14 major geomagnetic storms and they found a relationship between the hourly averaged magnitude of the  $B_z$  component of the IMF and the projected (expansion) speed,  $v$ , of CMEs launched from the central part of the solar disk. Thus, very fast CMEs with  $v > 1000$  km/s are capable of furnishing solar wind with negative magnetic fields of high intensities ( $B_z < 20$  nT) causing extremely intense storms, with the Dst index below  $-200$  nT.

Depending on the orientation of the magnetic field in an active region and the sign of magnetic helicity (magnetic twist), an earth directed CME may, or may not, be associated with a strong southward magnetic field component at 1AU and therefore it may, or may not, cause a geomagnetic storm. *Bothmer and Schwenn* [1994] and *Rust* [1994] showed that the twist and orientation of the magnetic field in filaments outside active regions correspond to twist and orientation of the magnetic fields in MCs. Later studies by *Bothmer and Rust* [1997], *Marubashi* [1997], *Zhao and Hoeksema* [1998], *Crooker* [2000], *McAllister and Martin* [2000] and *Ruzmaikin et al.* [2003] suggest that there is a straightforward relationship between the orientation of magnetic fields of erupted filaments and magnetic clouds. However, the situation seems to be different and less understood in the case of eruptions in active region. *Pudovkin et al.* [1977] concluded that the magnetic field in the main body of interplanetary ejecta is determined by the large-scale magnetic field of an active region, associated with the flare. *Tang et al.* [1985] reported that the orientation of  $B_z$  at 1AU may be in agreement with the flare field, opposite to it, or more often, fluctuating in both magnitude and direction. *Leamon et al.* [2002] reported that 46 MCs associated with active region sigmoids do not show the same high solar-terrestrial correlations as those associated with quiescent filaments. Earlier, *Pevtsov and Canfield* [2001] concluded that the magnetic structure of an individual active region plays a role in geomagnetic events, while *Leamon et al.* [2004] suggested that MCs, associated with active regions, are formed by reconnection between the active region and large-scale overlying magnetic fields. *Yurchyshyn et al.* [2001] found that directions of the helical magnetic fields in the leading edge of the magnetic clouds were consistent with the direction and helicity of the magnetic fields overlying the active region filaments. Potential magnetic field modeling by *Luhmann et al.* [2002; 2003] and *Zhao and Webb* [2003] suggest that the origin of CMEs is global and is related to the helmet streamer configurations which could be disturbed by the nearby evolving active regions. The above reports illustrate that our understanding of eruptions in active regions is obviously far from being complete: no single model of CMEs can satisfactorily explain the variety of eruptions in active regions and be successful in predicting the relationship between the solar magnetic fields and magnetic clouds.

In this paper we compare the magnetic fields in solar active regions of the October – November 2003 period and in corresponding interplanetary ejecta. We used space based data obtained by the Solar and Heliospheric Observatory (SOHO) and ground based data from the Big Bear Solar Observatory (BBSO) and Kanzelhöhe Solar Observatory (KSO) in Austria in order to study the orientations of the magnetic fields on the solar surface and at 1AU as well as to estimate parameters of the geomagnetic storms.

## 2. Solar flares in October – November 2003 and the associated geomagnetic activity

### 2.1. Solar Activity Overview

Three large sunspot regions have determined the level of solar activity over the period of time in October – November 2003. They produced many solar flares and CMEs (Figure 1), three of which caused significant disturbances in the earth's magnetosphere.

NOAA active region 0486 was located in the southern hemisphere and it launched a large number of X class flares<sup>1</sup>. The most powerful events were the X17.2 flare on October 28 and the X10

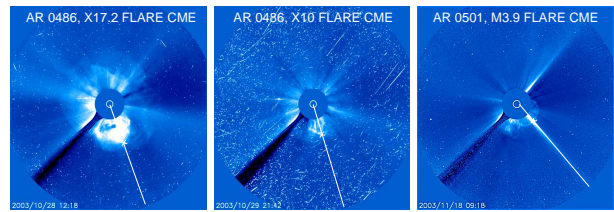


**Figure 1.** Most geoeffective solar coronal mass ejections observed by LASCO C3 in October – November 2003. The white line in each panel shows the position angle where the speed of the ejecta was measured. The white cross on the line marks the feature in the ejecta that was tracked for speed measurements.

flare on October 29. According to NOAA reports, the X17.2 flare erupted at 0951 UT on October 28 and a very fast earth directed CME was observed in conjunction with the flare. The fast moving October 28 CME was associated with a shock, which reached the earth at 0613 UT on October 29.

The X10 flare on October 29 erupted at 2037 UT and it was also accompanied by a very fast halo CME and an interplanetary shock that arrived at 1AU on October 30 at about 1700 UT.

NOAA active region 0484 grew rapidly as it passed across the solar disk and it produced only two weak X class flares. The same active region was observed again during the following solar rotation and it was classified as NOAA active region 0501. During the second passage, this active region gave rise to several medium sized M-class flares. However, one of them, the M3.9 flare on November 18 2003 at 0812UT, was associated with a fast halo CME which caused a major geomagnetic storm of the solar cycle 23 when the Dst index dropped below  $-470$ nT.

### 2.2. The X17.2 flare on October 28 2003

The X17.2 flare erupted in active region that was classified as a  $\delta$ -type magnetic configuration, which are known to produce strong flares [*Tian et al.*, 2002]. At the early stage of this long duration event two small flares, followed by eruptions, occurred in a

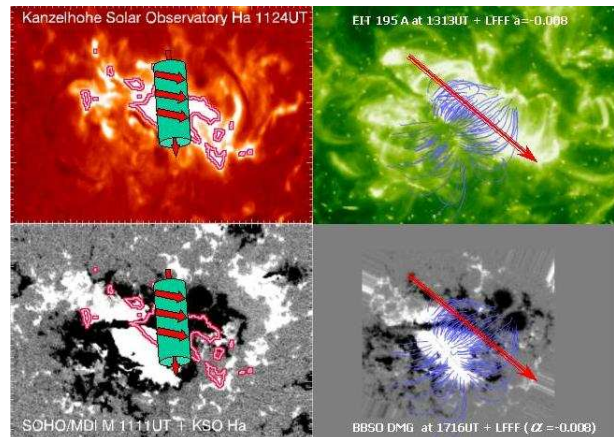


**Figure 2.** The X17.2 flare on October 28 2003. The upper left is an  $H\alpha$  image of the flare observed at Kanzelhöhe Solar Observatory at 1124 UT and the upper right panel is an EIT 195Å image at 1313UT. Lower panels show MDI (left) and BBSO (right) photospheric magnetograms. Over-plotted are: i) contours of the  $H\alpha$  flare (double red lines); ii) calculated magnetic force lines (thin blue lines); iii) direction of the axial field in the post-flare arcade on the sun (red arrow) and iv) directions of axial and azimuthal fields in the reconstructed MC (green cylinder and arrows).

quick succession. The impulsive phase of the major energy release started at about 1110 UT more than 1 hour after the beginning of the flare. Figure 2 shows flare images as observed in  $H\alpha$  (chromosphere),  $195\text{\AA}$  (corona) spectral lines as well as photospheric magnetograms. Double red contours show the position of the  $H\alpha$  flare, which was located at the major magnetic neutral line. The thin blue lines are magnetic force lines calculated from a linear force-free field (LFFF) model [Abramenko and Yurchishin, 1996a] with the parameter  $\alpha = -0.008 \text{ arcsec}^{-1}$ .

Negative LFFF parameter  $\alpha$  indicates that the post-flare arcade was left handed, i.e. it had negative helicity and the axial field of this arcade was directed approximately southwest (red arrow). Negative imbalance of current helicity ( $-15\pm 2\%$ ) calculated from BBSO vector magnetograms [Abramenko and Yurchishin, 1996b] as well as a reverse “S”  $H\alpha$  filament, observed prior to the flare,

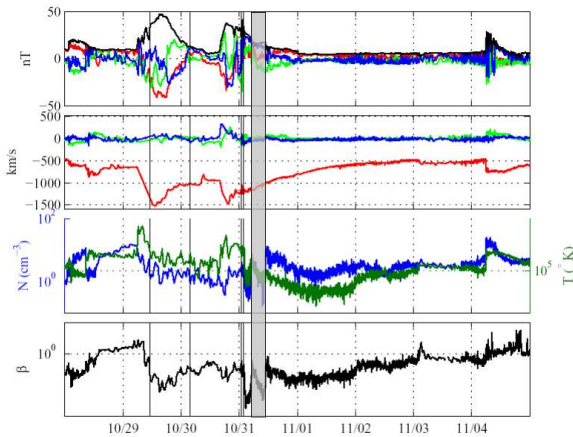


**Figure 4.** ACE data for October 29 – November 4, 2004. Two intervals, marked by the vertical lines, were used to reconstruct magnetic clouds on October 29 and October 30. Two top panels show time profiles for different components of the magnetic field and solar wind velocity ( $z$  - blue,  $y$  - green,  $x$  - red) and for the total magnetic field (top panel, black). The lower panels show speed of the ejecta, density, temperature and plasma  $\beta$ . Note the unusually high speeds of the ejecta exceeding 1000 km/s (red line in the second panel). Shaded interval shows a large scale structure with rotating  $B$ - $y$  magnetic component, which could not be reconstructed by Hu and Sonnerup technique.

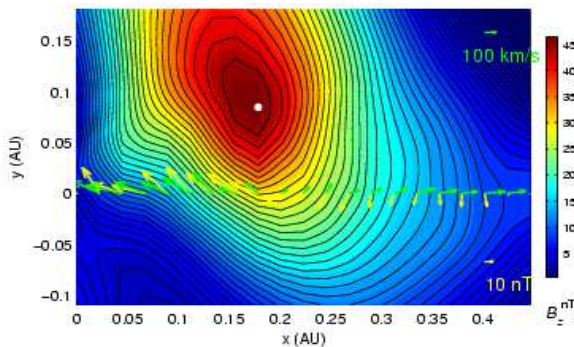


**Figure 5.** A cross-section of the October 29 MC associated with the October 28 CME. This MC was left handed (negative helicity) and its axial field was oriented nearly southward with the magnetic field peaking at 45 nT. Adopted from Hu et al. [2005].

both suggest that negative (left handed) magnetic twist dominated in the active region. Note that it is untypical for an active region located in the southern hemisphere to be left handedly twisted and often such “abnormal” active regions display increased level of flare activity [Tian et al., 2002].

The very fast and bright CME, associated with the flare, first appeared in the small field of view C2 of LASCO at 1130 UT. The CME had a two-part structure, which included a faint halo front and a bright dense core. The mean plane-of-sky speed of the halo front, measured at position angle (PA) of 92 degrees, where the leading edge moved fastest, was about 2125 km/s (PA is measured counter-clockwise from solar north in degrees). The mean speed of the bright core was considerably smaller and measured at about 1730 km/s at PA=195 deg (white line in the left panel of Figure 1).

According to magnetometer data taken by Advanced Composition Explorer (ACE), a large scale magnetic structure with a rotating magnetic field was observed between 1117 UT on October 29 and 0350 UT on October 30 (vertical lines in Figure 3) and it was identified as a magnetic cloud (a helical flux rope). This October 29 MC was reconstructed with a technique based on the Grad-Shafranov equation [Hu and Sonnerup, 2002; Hu et al., 2004]. The recovered cross-section of the flux rope is shown in Figure 4. The magnetic helicity of this MC was found to be negative, in agreement with the sign of the magnetic helicity of the active region, and the MC axis was pointed southward, i.e., the clock angle, measured clockwise from the  $y$ -axis of the GSE system was 266 degree. The error in the estimates of the cloud orientation is less than 6 degrees and it is determined by the maximum grid size used in the reconstruction. Note that this error does not affect the sign of magnetic helicity. The orientation of the MC at 1 AU can be mapped onto a magnetogram of the active region (green cylinder in Figure 2) which gives us the approximate orientation of the flux rope when it was launched from the sun, provided it was created in the solar corona and the orientation is preserved during propagation. Thus, Figure 2 (lower left panel) shows that the orientations of the MC, the axial field in the post-flare loop system and the neutral line generally agree and the difference between them is about 45 degrees.

### 2.3. The X10 flare on October 29 2003

Prior to the impulsive phase of the X10 flare, several bright patches were seen in  $H\alpha$  images taken at the Prairie View Solar Observatory (<http://www.pvamu.edu>), although the pre-event activity was significantly smaller as compared to that of the X17.2 flare.

This flare, too, was associated with the major magnetic neutral line and the flare emission was located to the east from the X17.2 flare observed the day before. A reverse “S” filament structure (Figure 5, upper right panel) was observed in the vicinity of the flare, which implies the presence of a left handed twist (negative helicity) in the magnetic system. The post-flare loop system too was left handed and its axial field was mainly northwardly directed (blue arrow in Figure 5).

A very fast halo CME accompanied the flare and it was first observed in the LASCO C2 field of view at 2054 UT as a moderately bright loop front over the south west limb. This CME, too, consisted of a faint halo front and a bright dense core (Figure 1, middle panel). The mean plane-of-sky speed of the halo, measured at PA=190 degrees where the leading edge moved fastest, was about 2029 km/s, while the mean speed of the bright core was considerably smaller and measured at about 1400 km/s at PA= 220 degree (white line in Figure 1, middle panel).

ACE data showed that a shock, presumably driven by the CME, arrived at 1 AU at about 1540 UT on October 30. Only one very short two hour long interval on October 31 (marked by two vertical solid lines) was found to which the Hu and Sonnerup technique could be applied. However, the reconstructed structure was too small and the uncertainties are too large to consider this structure to be an MC and to make any comparison with the solar surface data. Some indications on the presence of a larger structure could

be found, though, in the ACE time profiles between 0200 UT and 1100 UT on October 31 (shaded area). Within this time interval, the  $B_y$  component rotates from positive to negative (from East to West), while the  $B_z$  component remains positive (Northward directed) all the time. Such a behavior may indicate the presence of an ENW flux rope oriented mainly perpendicular to the ecliptic plane.

It is not clear whether the analyzed interval of ACE data and the second storm on October 30 are caused by the October 29 CME. However, it is interesting to point out that the axial field in this presumably left handed flux rope was directed northward, which coincides with the orientation and helicity of the post flare loop system and the magnetic neutral line.

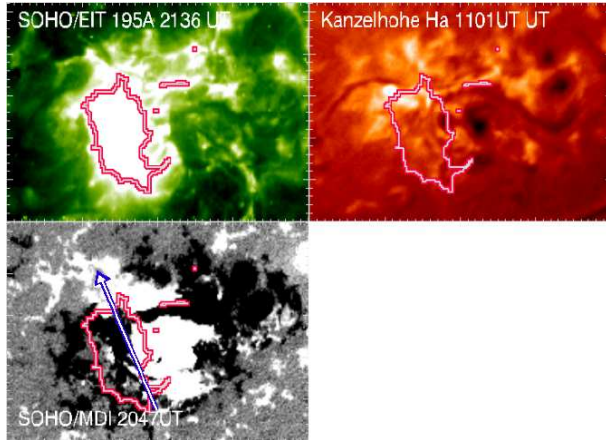


**Figure 3.** The X10 flare on October 29 2003. The upper left is an EIT 195Å image of the flare while a KSO H $\alpha$  image of the active region before the flare is shown in the upper right panel. The lower left panel shows an MDI longitudinal magnetogram. Double red contours mark the position of the EIT 195Å flare emission and the direction of the axial field in the post-flare arcade on the sun is shown by the blue arrow.

#### 2.4. The M3.9 flare on November 18 2003

The M3.9 flare was preceded by the activation and eruption of a dark filament seen in both H $\alpha$  and EIT 195Å spectral lines long before the flare (Figure 6, lower left panel). This filament did not reform after the eruption. During the main phase of the flare, the H $\alpha$  flare ribbons (red contours in Figure 6) stretched along the filament channel, while the post flare loop system covered only a small fraction of the flare ribbons. LFFF simulations with  $\alpha = 0.008$  arcsec $^{-1}$  showed that the axial field in this loop system was directed eastward and the magnetic field was positively twisted.

The associated CME first appeared in the LASCO C2 imager at 0850 UT as a wide faint loop above the southwest limb and it was first seen in LASCO C3 at 0918 UT (Figure 1, right panel). The shock, associated with the CME, arrived at 1AU at about 0730 UT on November 20 2003. [Dryer et al., 2004]. An MC was identified in the ejecta between 1011 UT and 1943 UT (Figure 7, vertical solid lines) and reconstructed with the Hu and Sonnerup technique. The recovered cross-section of the flux rope is shown in Figure 8. Magnetic helicity of the MC was positive, in agreement with the sign of the helicity determined for the post-flare loop system, associated with this CME. The axis of this MC was pointed southeast (clock angle was about 311 deg) and its orientation was mapped onto the active region (green cylinder in Figure 6), which showed that the directions of the axial field in the MC and the post-flare loop system (blue arrows) differ by about 50 degrees.

It is interesting to note the following fact. We made an attempt to identify the footpoints of this filament and they are indicated by the white arrows in the 0713 UT EIT 195Å image (Figure 6, lower left). Strikingly, the line connecting the footpoints has an orientation similar to that of the MC at 1AU. If our identification is correct,

then the MC was, quite possibly, the result of the eruption of a pre-existing flux rope, as described by flux rope models [Forbes and Isenberg 1991; Wu et al., 1999; Amari et al., 2000]. Furthermore, the positive twist of both the MC and the post flare loop system may imply that the erupted filament was probably of the inverse polarity configuration [Low 2001], otherwise, the MC should have been left handed, i.e., it would have negative helicity.

Gopalswamy et al. [2005] analyzed the same event and their results seem to support the suggestion about the association between the MC and the erupted filament. However, the static force-free flux-rope fitting, used in their study, produced an MC more inclined toward the ecliptic plane (287 deg) than the MC found in this study (311 deg). They further suggest that the MC was associated with the largest north-south segment of the erupted filament.

### 3. Magnitude of the geomagnetic storms as estimated from the projected speed CMEs

As we mentioned earlier, the speed of the CMEs, measured near the sun immediately after the eruption, is correlated with the magnetic field in the associated ejecta [Yurchyshyn et al., 2003; 2004] and the peak value of the Dst index [Yurchyshyn et al., 2003; 2004; Gonzalez et al., 2004; Srivastava and Venkatakrishnan 2004]. Thus, the above results may provide us with a capability to estimate the magnitude of the IMF in an ejecta and the intensity of the corresponding geomagnetic storm based on the speed of the CME. Because the speed can be measured from LASCO images immediately after the eruption, such estimates can be obtained 1 – 2 day prior to the onset of geomagnetic activity and, thus, can be used to forecast space weather.

We determined the projected speeds of the three CMEs and used them as an input parameter for three different methods to estimate the intensity of the resulting geomagnetic storms.

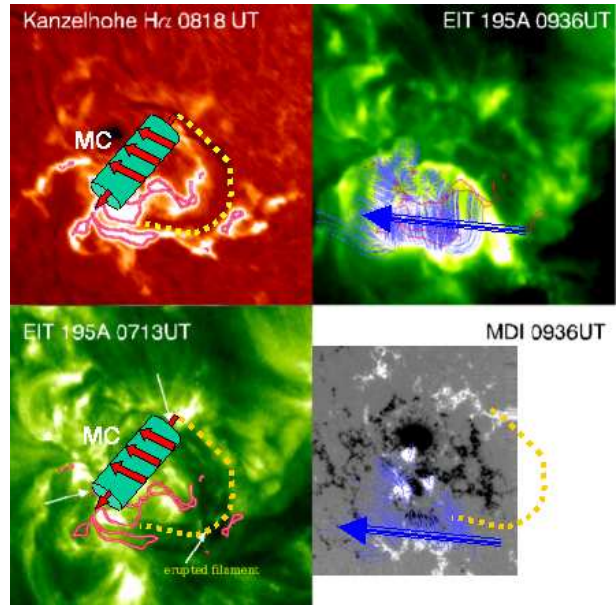


**Figure 6.** KSO H $\alpha$  (upper left) and EIT 195Å (upper right and lower left) images of the M3.9 flare on November 18, 2003. MDI magnetogram for NOAA AR 0501 is shown in the lower right panel. The erupted filament is indicated by yellow dots. The double red contours show the position of the H $\alpha$  flare. Over-plotted also are magnetic field lines calculated from a LFFF model (blue lines) and the direction of the axial magnetic field in the observed post flare arcade (blue arrow) and in the associated MC at 1AU (green cylinder).

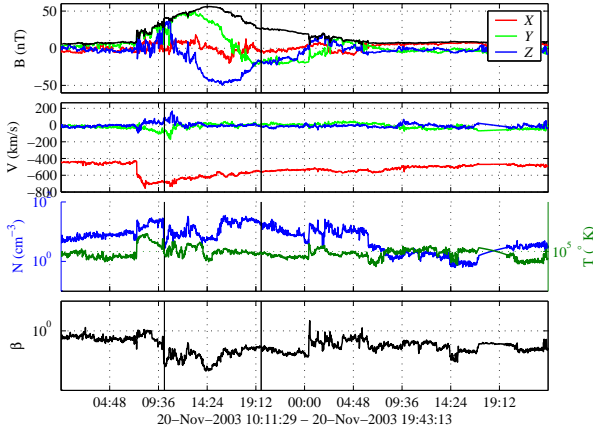
### 3.1. CME speed measurements

Figure 1 shows several of the October – November CMEs at the early phase of their development. The white solid lines mark the position angle at which we measured the projected speed of each event and the crosses on the white lines mark the features of the CMEs, which we used to measure the projected speed.

In general, the bright core, seen in the structure of the CMES, is thought to be located at the bottom of the erupting flux rope, which is often observed at 1AU as an MC. Because we are mainly interested in the speed of the flux rope rather than the speed of the interplanetary shock, we tracked the leading edge of these dense cores instead of the faint halos.

### 3.2. Method I

*Yurchyshyn et al.* [2003, 2004] analyzed 14 major geomagnetic storms and reported on the relationship between the hourly aver-



**Figure 7.** ACE data for November 20, 2003 event. A large scale structure between 1012 UT and 1943 UT, marked by the vertical lines, was identified as an MC and the data for this time interval were used to reconstruct the shape and the orientation of this MC. Note the smoothly rotation  $B-y$  component in this magnetic structure. The MC which was right handed and oriented nearly along the NW-SE line with the axial field pointing southeast (red arrow in Figure 6). Two top panels show time profiles for different components of the magnetic field and solar wind velocity ( $z$  - blue,  $y$  - green,  $x$  - red) and for the total magnetic field (top panel, black). The lower panels show time profiles for density, temperature and plasma  $\beta$  in the ejecta.

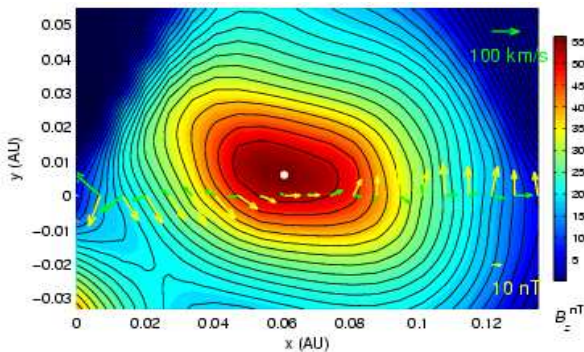


**Figure 8.** A cross-section of the November 20 MC associated with the November 18 CME. This MC was right handed (positive helicity) and its axial field was inclined toward the ecliptic plane by about 50 degree.

aged magnitude of the  $B_z$  component of the IMF (GSM system) and the projected speed,  $v$ , of CMEs. Since then, 15 more events were added to the data set and the end result is presented in Figures 9 – 10. According to Figure 9, the hourly averaged magnitude of the southward component  $B_z$  can be estimated from the projected speed of the CME,  $v$ , based on the following equation

$$B_z(nT) = 9.3 + 0.6 \exp(v/404), \quad (1)$$

where  $v$  is measured in km/s. Generally speaking, an interplanetary ejecta can assume any orientation in space, therefore, the strength of its southward component in the GSM coordinate system depends on the inclination angle relative to the earth's magnetic axis. To take into account of this uncertainty, in Figure 10 we plot the peak magnitude of the total magnetic field in an ejecta,  $B_t$ , versus the projected speed for the same events as in Figure 9. In this case, the best fit to the data points is slightly different

$$B_t(nT) = 13.4 + 0.6 \exp(v/404), \quad (2)$$

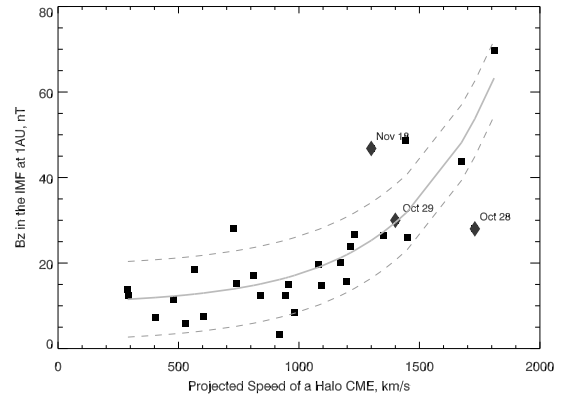


**Figure 9.** The absolute peak values of the  $B_z$  component plotted versus the projected speed of CMEs. The solid line is an exponential fit to the data points. The dashed lines show the extent of the error to this fit. Diamonds show data for the events discussed in this study.

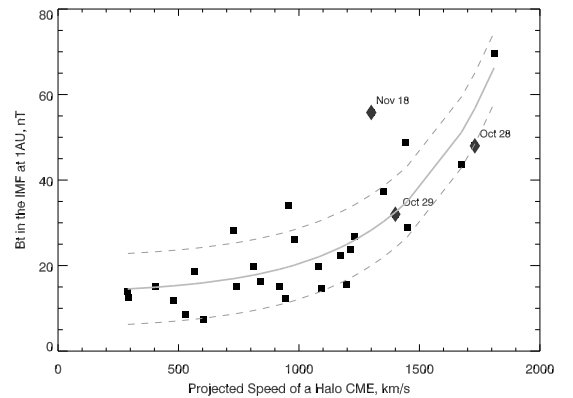


**Figure 10.** The peak values of the total magnetic field in ICMEs plotted versus the projected speed of CMEs. The solid line is an exponential fit to the data points. The dashed lines show the extent of the error to this fit. Diamonds show data for the events discussed in this study.

and it can be used to estimate the upper bound for the  $B_z$  assuming that the southward component is made up entirely of the total field  $B_t$ , and the  $B_x$  and  $B_y$  components are small compared to  $B_z$ . This is possible only when the MC is oriented parallel ( $B_z =$  azimuthal field) or perpendicular ( $B_z =$  axial field) to the ecliptic plane. The last step in the prediction scheme is to estimate the intensity of the geomagnetic storm as described in *Yurchyshyn et al.* [2004]:

$$Dst = -2.846 + 6.54B_z - 0.118B_z^2 - 0.002B_z^3, \quad (3)$$

where  $B_z$  and the Dst index are measured in nT.

### 3.3. Method II

*Gonzalez et al.* [2004] studied 13 magnetic clouds and they proposed that the peak intensity of a geomagnetic storm (peak Dst), caused by magnetic clouds, can be directly predicted from the expansion (projected) speed of a halo CME,  $v$ , measured near the sun by using the following equation:

$$Dst = 5.2 \times 10^{-4} (0.22v + 340)^2. \quad (4)$$

### 3.4. Method III

This last method is a combination of several independent studies. *Owens and Cargill* [2002] reported on the relationship between the maximum field magnitude in an ejecta (both MCs and structures without field rotation),  $B_t$ , and its maximum speed,  $v$ , near 1AU:

$$B_t(\text{nT}) = 0.047v + 0.644. \quad (5)$$

They also found that this maximum speed is related to the transit time of a CME from the sun to the satellite:

$$t(\text{days}) = -0.0042v + 5.14. \quad (6)$$

There are several different models to estimate the transit time/shock arrivals at 1AU (see *Dryer et al.* [2004] for a review of their performance during the ‘‘Halloween 2003 epoch’’). However, for our purposes we used an empirical relationship between the initial speed of a CME and the travel time reported by *Goplaswamy et al.* [2000] (see Figure 3 in this article). Thus, in this prediction scheme we will first estimate the transit time, then the speed of the ejecta and the peak value of the magnetic field at 1AU. As the final step, the peak value of the Dst index will be determined from equation (3) assuming that the ejecta is oriented in such a way that its  $B_z$  component equals the maximum field,  $B_t$ , determined from equation (5).

**Table 1.** Predicted and observed parameters of MCs and geomagnetic storms

	$B_z$ , nT	Dst( $B_z$ ), nT	$B_t$ , nT	Dst( $B_t$ ), nT
Oct 28 CME, $v=1730$ km/s				
Method I	-46 ... -60	-313 ... -379	50 ... 64	-316 ... -382
Method II	—	-200 ... -300	—	—
Method III	—	—	40 ... 54	-299 ... -365
Obs	-28	-308(-308)	48	-308(-308)
Oct 29 CME, $v=1400$ km/s				
Method I	-21 ... -35	-189 ... -255	25 ... 39	-218 ... -284
Method II	—	-170 ... -270	—	—
Method III	—	—	38 ... 52	-290 ... -356
Observed	-30	-347(-295)	38	-347(-295)
Nov 18 CME, $v=1300$ km/s				
Method I	-17 ... -31	-156 ... -222	21 ... 35	-187 ... -253
Method II	—	-150 ... -250	—	—
Method III	—	—	33 ... 47	-266 ... -332
Observed	-52	-472(-440)	56	-472(-440)

## 3.5. Results

In Table I we show the estimates for the strength of the IMF in the ejecta and the magnitude of the geomagnetic storms and compare them to the observed values. In the 1st and 2nd columns we show the calculated values for  $B_z$  and the Dst index determined from this  $B_z$ . The 3rd and 4th columns are estimates for the total field  $B_t$  and for the upper bound of the Dst index, assuming that this Dst index was associated with a  $B_z$  component made up entirely from the  $B_t$ . In the table row ‘‘observed’’ we list  $B_z$  and  $B_t$  as measured by the ACE magnetometer and the Dst index as provided by the World Data Center for Geomagnetism in Kyoto (Japan). The first number for the Dst is the lowest value registered, while the number in parenthesis is the change of the Dst index relative to the pre-storm base value.

In general, the estimated numbers obtained by the three methods differ, however they all more or less correctly ‘‘predicted’’ the magnitude of the October 29 and October 30 storms and they all missed by a lot while predicting the November 20 geomagnetic storm.

Method II underestimated, by a different degree, the Dst index for all events and generated no estimates for the strength of the magnetic field. The combined Method III produced correct numbers for both the total field  $B_t$  and the changes in the Dst index in two out of three cases (October 28 and October 29). Method I was successful in the estimating  $B_z$  and  $B_t$  for the October 29 event. It also was very close in ‘‘predicting’’  $B_t$  for the October 28 CME, though,  $B_z$  was significantly underestimated. As to the Dst index, Method I produced either slightly over (October 28 event) or under (October 29) estimated values (see also Figures 9 and 10, diamonds).

Although the speed of the November 18 CME was not as large as in the October events, the corresponding geomagnetic storm was quite remarkable. The key reason for this severe storm was an unusually strong magnetic field within the MC. The orientation of the MC was also favorable in a way that its  $B_z$  component was almost entirely made up of the MC’s axial field (compare the black and the blue lines in the top panel of Figure 7), which was mainly pointed southward. The large field strength in this MC could be a cumulative effect of several different factors: i) compression at the front edge due to the difference between the speed of the MC and the upstream speed, although the reconstructed cross-section of this MC does not show such compression; ii) interaction with another CME which erupted earlier and iii) ‘‘solar factor’’, i.e. the magnitude of the magnetic field in this flux rope was pre-determined by magnetic fields in NOAA active region 0501.

## 4. Concluding Remarks

The study, presented here, further supports earlier findings that the CME speed appears to be associated with the strength of the IMF and thus the magnitude of a geomagnetic storm. It was also found that directions of the helical magnetic fields in magnetic clouds on October 29 and November 20, and less evident on the October 30, were consistent with the direction and helicity of the magnetic fields in the source active regions.

These findings are quite significant in terms of their potential to predict severity of geomagnetic activity. Measurements of the velocity and the orientation of the erupted solar fields could provide quantitative estimations of the intensity of  $B_z$  and the orientation of the interplanetary magnetic field 1 – 2 days in advance, immediately after the earth directed solar eruption occurred on the sun. The prediction scheme uses readily available ground and space based solar data and thus it may be easily implemented for space weather forecast.

### Acknowledgments.

We thank reviewers for their comments and criticism which led to a significant improvement of the manuscript. We also thank the ACE MAG instrument team and the ACE Science Center for providing the ACE data. We acknowledge the use of geomagnetic data from the World Data Center for Geomagnetism in Kyoto. The CME catalog is generated, and maintained,

by the Center for Solar Physics and Space Weather, The Catholic University of America in cooperation with the Naval Research Laboratory and NASA. SOHO is a project of international cooperation between ESA and NASA. We are obliged to BBSO staff for their effort in obtaining the data. This work was supported, in part, by NSF grants ATM-9903515, ATM-0205157, ATM-0076602 and NASA (NAG5-9682) and NNG04GF47G grants.

## Notes

1. Solar flares are classified according to the peak X-ray flux emitted in the wavelength range of 1 to 8 Å. X flares are major energy release events that can trigger long lasting geomagnetic storms; M-class flares are moderately strong and C-class flares are small. An X1.0 flare is 10 times stronger than an M1.0 flare. See <http://www.spaceweather.com/glossary/flareclasses.html> for more details

## References

Abramenko, V.I., and V.B. Yurchishin (1996a), Modeling of a linear force-free magnetic field in a bounded domain, *Solar Phys.*, *168*, 47.

Abramenko, V.I., and V.B. Yurchishin (1996b), Analysis of electric current helicity in active regions on the basis of vector-magnetograms, *Solar Phys.*, *168*, 75.

Amari, T., J.F. Luciani, Z. Mikic, and J. Linker (2000), A twisted flux rope model for coronal mass ejections and two-ribbon flares, *Astrophys. J.*, *529*, L49.

Barbieri, L.P., and R.E. Mahmot (2004), October - November 2003's space weather and operations lessons learned, *Space Weather*, *2*, S09002, doi:10.1029/2004SW000064.

Bothmer, V., and R. Schwenn (1994), Eruptive prominences as sources of magnetic clouds in the solar wind, *Space Sci. Rev.*, *70*, 215.

Bothmer, V., and D.M. Rust (1997), in *Coronal Mass Ejections*, Geophysical Monograph 99, ed. N. Crooker, J.A. Joselyn, & J. Feynman, Washington, DC: AGU, 139

Bothmer, V., and R. Schwenn (1998), The structure and the origin of magnetic clouds in the solar wind, *Ann. Geophysicae*, *16*, 1.

Burlaga, L. F., E. Sittler, F. Mariani, and R. Schwenn (1981), Magnetic loop behind an interplanetary shock - Voyager, Helios, and IMP 8 observations, *J. Geophys. Res.*, *86*, 6673.

Burlaga, L. F., R.M. Skoug, C.W. Smith, D.F. Webb, T.H. Zurbuchen, A. Reinard (2001), Fast ejecta during the ascending phase of solar cycle 23: ACE observations, 1998-1999, *J. Geophys. Res.*, *106*, 20957.

Cane, H.V., I.G. Richardson, and O.C. St. Cyr (2000), Coronal mass ejections interplanetary ejecta and geomagnetic storms, *Geophys. Res. Lett.*, *27*, 3591.

Crooker, N.U. (2000), Solar and heliospheric geoeffective disturbances, *J. Atmos. Sol. Terr. Phys.*, *62*, 1071.

Dal Lago, A., W.D. Gonzalez, A.L.C. de Gonzalez, L.E.A. Vieira (2001), Compression of magnetic clouds in interplanetary space and increase in their geoeffectiveness, *J. Atm. Sol. Terr. Phys.*, *63*, 451.

Dryer, M., Z. Smith, C.D. Fry, W. Sun, C.S. Deehr, S.-I. Akasofu (2004), Real-time shock arrival predictions during the 'Halloween 2003 epoch', *Space Weather*, *2*, No. 9, S09001, 10.1029/2004SW000087.

Dryer, M. (1994), Interplanetary Studies: Propagation of Disturbances Between the Sun and the Magnetosphere, *Space Sci. Rev.*, *67*, 363.

Dungey, J.W. (1961), Interplanetary magnetic field and the auroral zones, *Phys. Res. Lett.*, *6*, 47.

Forbes, T.G., and P.A. Isenberg (1991), A catastrophe mechanism for coronal mass ejections, *Astrophys. J.*, *373*, 294.

Howard, R. A., D.J. Michels, N.R. Sheeley Jr, and M.J. Koomen (1982), The observation of a coronal transient directed at earth, *Astrophys. J.*, *263*, L101.

Hu, Q., and B.U.Ö. Sonnerup (2002), Reconstruction of magnetic clouds in the solar wind: Orientations and configurations, *J. Geophys. Res.*, *107*, doi 10.1029/2001JA000293.

Hu, Q., C. W. Smith, N. F. Ness, and R. M. Skoug (2005), On the magnetic topology of October/November 2003 events, *J. geophys. Res.*, in press

Gonzalez, W.D., and B.T. Tsurutani (1987), Criteria of interplanetary parameters causing intense magnetic storms (Dst < 100 nT), *Planet. Space Sci.*, *35*, 1101.

Gonzalez, W.D., J.A. Joselyn, Y. Kamide, H.W. Kroehl, G. Rostoker, B.T. Tsurutani, and V.M. Vasyliunas (1994), What is a geomagnetic storm? *J. Geophys. Res.*, *99*, 5771.

Gonzalez, W.D., A. Dal Lago, A.L. Clúa de Gonzalez, L.E.A. Vieira, and B.T. Tsurutani (2004), Prediction of peak-Dst from halo CME/magnetic cloud speed observations, *J. Atm., Sol. Terr. Phys.*, *66*, 161.

Gopalswamy, N., A. Lara, R.P. Lepping, M.L. Kaiser, D. Berdichevsky, and O.C. St. Cyr (2000), Interplanetary acceleration of coronal mass ejections, *Geophys. Res. Lett.*, *27*, 145.

Gopalswamy, N., S. Yashiro, G. Michalek, H. Xie, R.P. Lepping, and R.A. Howard, (2005), Solar source of the largest geomagnetic storm of cycle 23, *Geophys. Res. Lett.*, accepted.

Gosling, J.T., E. Hildner, R.M. MacQueen, R.H. Munro, A.I. Poland, and C.L. Ross (1974), Mass ejections from the sun - A view from SKYLAB, *Astrophys. J.*, *79*, 4581.

Leamon, R.J., R.C. Canfield, and A.A. Pevtsov (2002), Properties of magnetic clouds and geomagnetic storms associated with eruption of coronal sigmoid, *J. Geophys. Res.*, *107*, doi 10.1029/2001JA000313.

Leamon, R.J., R.C. Canfield, S.L. Jones, K. Lambkin, B.J. Lundberg, and A.A. Pevtsov (2004), Helicity of magnetic clouds and their associated active regions, *J. Geophys. Res.*, *109*, CiteID A05106.

Lindsay, G.M., J.G. Luhmann, C.T. Russell, and J.T. Gosling (1999), Relationship between coronal mass ejection speeds from coronagraph images and interplanetary characteristics of associated interplanetary coronal mass ejections, *J. Geophys. Res.*, *104*, 12515.

Low, B.C. (2001), Coronal Mass ejections, magnetic flux ropes, and solar magnetism, *J. Geophys. Res.*, *106*, 25141.

Luhmann, J.G., Y. Li, C.N. Arge, X.-P. Zhao, Y. Liu, O.C. St. Cyr, and N. Rich (2002), Using Potential Field Models to Learn About CME Coronal Context and Consequences, 200th AAS Meeting, BAAS, *34*, #65.06, 751.

Luhmann, J.G., Y. Li, X. Zhao, and S. Yashiro (2003), Coronal Magnetic Field Context of Simple CMEs Inferred from Global Potential Field Models, *Solar Phys.*, *213*, 367.

MacQueen, R. M., J. A. Eddy, J.T. Gosling, E. Hildner, R.H. Munro, G.A.Jr Newkirk, A.I. Poland, and C.I. Ross (1974), The Outer Solar Corona as Observed from Skylab: Preliminary Results, *Astrophys. J.*, *187*, L85.

Marubashi, K. (1997), Interplanetary Magnetic Flux Ropes and Solar Filaments, in *Coronal Mass Ejections*, Geophysical Monograph 99, ed. N. Crooker, J.A. Joselyn, and J. Feynman (Washington, DC: AGU), 147.

McAllister, A. H., M. Dryer, P. McIntosh, H. Singer, and L.A. Weiss (1996), A large polar crown coronal mass ejection and a 'problem' geomagnetic storm: April 14-23, 1994, *J. Geophys. Res.*, *101*, 13497.

McAllister, H., and S.F. Martin (2000), The essential role of magnetic reconnection in erupting prominences and CMEs, *Adv. Space Res.*, *26*, 469.

Owens, M.J., and P.J. Cargill (2002) Correlation of magnetic field intensities and solar wind speeds of events observed by ACE, *J. Geophys. Res.*, *107*, 1050.

Pevtsov, A.A., and R.C. Canfield (2001), Solar magnetic fields and geomagnetic events, *J. Geophys. Res.*, *106*, 25191.

Pudovkin, M.I., S.A. Zaitseva, I.P. Oleferenko, and A.D. Chertkov (1977), The structure of the solar flare stream magnetic field, *Solar Phys.*, *54*, 155.

Rostoker, G. and C.-G. Falthammer (1967), Relationship between changes in the interplanetary magnetic field and variations in the magnetic field at the Earth's surface, *J. Geophys. Res.*, *72*, 5853.

Russell, C.T., R.L. McPherron, and R.K. Burton (1974), On the cause of geomagnetic storms, *J. Geophys. Res.*, *79*, 1105.

Rust, D.M. (1994), Spawning and shedding helical magnetic fields in the solar atmosphere, *Geophys. Res. Lett.*, *21*, 241.

Ruzmaikin, A., S.F. Martin, and Q. Hu (2003), Signs of magnetic helicity in interplanetary coronal mass ejections and associated prominences: Case study, *J. Geophys. Res.*, *108*, 1096, doi:10.1029/2002JA009588

Srivastava, N., and P. Venkatakrishnan (2004), Solar and interplanetary sources of major geomagnetic storms during 1996-2002, *J. Geophys. Res.*, *109*, CiteID A1010, doi: 10.1029/2003JA010175.

Tang, F., S.-I. Akasofu, E. Smith, B. Thsurutani (1985), Magnetic fields on the sun and the north-south component of transient variations of the interplanetary magnetic field at 1 AU *J. Geophys. Res.*, *90*, 2703

Tian, L., Y. Liu, and J. Wang (2002), The most violent super-active regions in the 22nd and 23rd cycles, *Solar Phys.*, *209*, 361.

Tousey, R. (1973), The solar corona, in *COSPAR Space Research*, *XIII*, 713.

Wilson, R.M., and E. Hildner (1984), Are interplanetary magnetic clouds manifestations of coronal transients at 1 AU? *Solar Phys.*, *91*, 169.

Wu, S. T., W.P. Guo, D.J. Michels, and L.F. Burlaga (1999), MHD description of the dynamical relationships between a flux rope, streamer, coronal mass ejection, and magnetic cloud: An analysis of the January 1997 Sun-Earth connection event, *J. Geophys. Res.*, *104*, 14789.

Wu, C.C., and R.P. Lepping (2002), The effect of solar wind velocity on magnetic cloud-associated magnetic storm intensity, *J. Geophys. Res.*, *107*, 1346.

- Wu, C.C., and R.P. Lepping (2005), Relationships for predicting magnetic cloud-related geomagnetic storm intensity, *J. Atm. Sol.-Terr. Phys.*, *67*, 283.
- Yurchyshyn, V.B., H. Wang, P.R. Goode, and Y. Deng (2001), Orientation of magnetic fields in interplanetary flux ropes and solar filaments, *Astrophys. J.*, *563*, 381.
- Yurchyshyn V., H. Wang, and V. Abramenko (2003), How directions and helicity of erupted solar magnetic fields define geoeffectiveness of coronal mass ejections, *Adv. Space Res.*, *32*, 1965.
- Yurchyshyn, V., H. Wang, V. Abramenko (2004), Correlation between speeds of CMEs and the intensity of geomagnetic storms, *Space Weather*, *2*, S02001, doi:10.1029/2003SW000020.
- Zhao, X.P., and J.T. Hoeksema (1998), Central axial field direction in magnetic clouds and its relation to southward interplanetary magnetic field events and dependence on disappearing solar filaments, *J. Geophys. Res.*, *103*, 2077.
- Zhao, X.P., and D.F. Webb (2003), Source regions and storm effectiveness of frontside full halo coronal mass ejections, *J. Geophys. Res.*, *108*, 1234.

---

<sup>1</sup>Big Bear Solar Observatory, Big Bear City, CA 92314, USA

<sup>2</sup>IGPP, University of California, Riverside, CA 92521, USA

<sup>3</sup>Crimean Astrophysical Observatory, Crimea, Ukraine